Mechanism of bistability: Tonic spiking and bursting in a neuron model

Andrey Shilnikov*
Department of Mathematics and Statistics, Georgia State University, Atlanta, Georgia 30303, USA

Ronald L. Calabrese
Biology Department, Emory University, Atlanta, Georgia 30322, USA

Gennady Cymbalyuk
Department of Physics and Astronomy, Georgia State University, Atlanta, Georgia 30303, USA
(Received 30 March 2004; revised manuscript received 16 July 2004; published 31 May 2005)

Neurons can demonstrate various types of activity; tonically spiking, bursting as well as silent neurons are frequently observed in electrophysiological experiments. The methods of qualitative theory of slow-fast systems applied to biophysically realistic neuron models can describe basic scenarios of how these regimes of activity can be generated and transitions between them can be made. Here we demonstrate that a bifurcation of a codimension one can explain a transition between tonic spiking behavior and bursting behavior. Namely, we argue that the Lukyanov-Shilnikov bifurcation of a saddle-node periodic orbit with noncentral homoclinics may initiate a bistability observed in a model of a leech heart interneuron under defined pharmacological conditions. This model can exhibit two coexisting types of oscillations: tonic spiking and bursting, depending on the initial state of the neuron model. Moreover, the neuron model also generates weakly chaotic bursts when a control parameter is close to the bifurcation values that correspond to homoclinic bifurcations of a saddle or a saddle-node periodic orbit.

DOI: 10.1103/PhysRevE.71.056214 PACS number(s): 05.45.Ac, 05.45.Pq, 87.19.La, 02.40.Xx

I. INTRODUCTION

Neurons are observed in one of three fundamental, generally defined modes: silence, tonic spiking, and bursting. The functional role of bursting has been actively discussed in recent theoretical and experimental studies. There is agreement that it is an important mode for control of rhythmic movements and is frequently observed in central pattern generators and neuronal networks controlling motor behavior [1]. Also, bursting has been widely observed in sleep and pathological brain states [2]. More recently, bursting has begun to be identified with other functions. It has been proposed to improve reliability of memory formation [3,4]. Neurons in bursting mode differ in their ability to transmit information and respond to stimulation from those in tonic spiking mode and appear to play an important role in information transfer and processing in normal states of the nervous system [5,6]. The coexistence of bursting and tonic spiking modes, as well as that of different bursting modes with each other, has been observed in modeling [7–11] and experimental [12–14] studies and this complexity adds potential flexibility to the nervous system. Such multistability may be controlled by neuromodulators and thus reflect the functional state of the nervous system. Multistability has many potential implications for dynamical memory and information processing in a neuron [7,8,14–16].

A mathematical model of a single neuron is to demonstrate regimes similar to those observed in experiments. Besides, variations of certain biophysical parameters in the model may cause proper transitions between these regimes. Depending on initial conditions or perturbations these regimes may co-exist within certain parameter ranges. Bursting behavior has been well described within a framework of the methods of qualitative theory of slow-fast systems; see comprehensive reviews in [17–19]. Of special interest are various mechanisms of transitions between tonic spiking and bursting [20–24]. Some transitions are associated with the chaotic behavior, which is due to the shift dynamics arising near a homoclinic bifurcation of a saddle (or saddle-focus) point of a singularly perturbed system [22,23,25]. Here, we report a new, distinct scenario where the bifurcation underlying the transition from tonic spiking into bursting is homoclinic as well, but in distinction, it employs a saddle or a saddle-node periodic orbit rather than saddle equilibria. This mechanism explicates a *smooth transition* between the tonic spiking and bursting activities of the neuron.

Bistability means the coexistence of a pair of attractors separated in the phase space [37]. We describe a global bifurcation of a saddle-node periodic orbit with homoclinic orbits, which provides an explanation for this phenomenon. Such a saddle-node periodic orbit is sketched in Fig. 1. Namely, after it splits into a stable periodic orbit and a saddle one in the phase space, the stable manifold of the latter can separate the attraction basin of the bursting from that of a stable periodic orbit representing the tonic spiking. Furthermore, we identify a physiologically plausible parameter in the model (1) that can control duration of a burst, the time interval between the first and last spikes in the burst.

In the paper, first we introduce a model of a single leech neuron. Then we develop a general geometrical framework for the analysis of periodic solutions of slow-fast dynamical systems. It allows us to give a general phenomenological

*Electronic address: ashilnikov@mathstat.gsu.edu

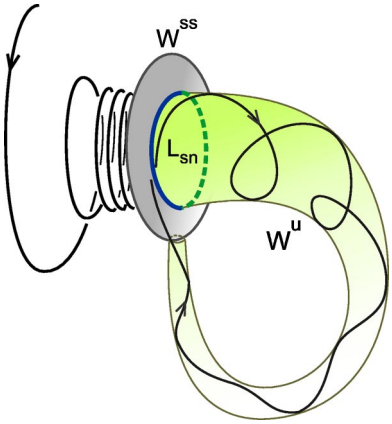

FIG. 1. (Color online) Saddle-node periodic orbit L_{sn} with noncentral homoclinics: the unstable manifold W^u comes back to L_{sn} crossing transversally the nonleading manifold W^{ss}. The latter separates the node region (from the right of W^{ss}) where the periodic orbit L_{sn} is stable from the saddle region containing the unstable manifold W^u comprised of the trajectories converging to L_{sn} as time tends to $-\infty$.

description for the Lukyanov-Shilnikov bifurcation of a saddle-node periodic orbit with noncentral homoclinics in these systems. We show how this bifurcation creates a bistability in a generic neuron model. Throughout the presentation we draw parallels between the phenomenological description and the accurate numerical bifurcation analysis of the model of the single leech neuron. The developed technique is applicable to a broad class of neuron models. Our results make feasible predictions for future experimental studies.

II. NEURON MODEL

A bursting regime reflects complexity in the dynamics of various membrane ionic currents, operating at different time scales. The ionic currents are commonly quantified through voltage-clamp experiments and modeled according to a formalism introduced by Hodgkin and Huxley [26]. A complete neuron model, including all currents identified experimentally, is rather complex for thorough studies.

The relatively small number of neurons in invertebrate nervous systems and the possibility to identify most of them from preparation to preparation all make these identifiable neurons attractive for the dynamical systems analysis. Here we exploit identified oscillator interneurons that are part of the leech heartbeat central pattern generator.

When isolated pharmacologically from the rest of the network these neurons show autonomous bursting behavior [27]. In these neurons, eight voltage-dependent ionic currents have been well identified and characterized (see [28,29] and references therein). Classified by their ionic specificity, these currents are separated in four groups. The first group consists of two sodium currents: a fast sodium current (I_{Na}) and a persistent sodium current (I_{NaP}). The second group consists of three potassium currents: a delayed rectifierlike potassium current (I_{K1}), a persistent potassium current (I_{K2}), and a fast transient potassium (I_{Ka}). The third group consists of two low-threshold calcium currents: one rapidly (I_{CaF}) and one slowly inactivating (I_{CaS}). The last group consists of a single current, carried by both sodium and potassium: a hyperpolarization-activated current (I_h). All these currents, except for the fast sodium current, were quantified in voltage clamp experiments [29]. The model equations for I_{Na} current were borrowed from the original work by Hodgkin and Huxley adjusted for leech kinetics. None of these currents is dependent on the intracellular concentration of any particular ion. A canonical model of a single neuron has been constructed and tuned to reproduce experimentally observed behaviors [27]. It consists of 14 ordinary differential equations running at multiple time scales which vary from a few milliseconds through seconds. As alluded to above, a comprehensive analysis of this model would be quite difficult and challenging.

Blockade of groups of currents in living heart interneurons simplifies neuronal dynamics and elicits characteristic behaviors. These characteristic behaviors present interesting phenomena for study from the perspective of the theory of dynamical systems. One of the commonly observed characteristic behaviors is observed under blockade of Ca^{2+} currents. In leech neurons, application of divalent ions like Co^{2+}, which block Ca^{2+} currents, along with partial block of outward currents, elicits slow plateaulike oscillations with a period up to 60 s and plateau duration up to 20 s. This phenomenon persists after a blockade of I_h.

Previously, in our modeling studies [11], we addressed the question of how these slow temporal characteristics are produced by a system with dynamics based on much faster time scales (time constants of the ionic currents involved do not exceed 1 s). We derived a simplified neuron model by taking into account that the experimental conditions eliminated or reduced the contribution of certain currents to the dynamics of the neuron. This simplified model, based on the dynamics of I_{Na} and I_{K2} currents, is described as a system of three differential equations. We showed that the classical model of the transient Na^+ current is sufficient for the generation of long plateau behavior due to the properties of a window current (a transient Na^+ current can be a persistent "window" current in a certain range of membrane potential values). The simplified model (1) can also produce slow plateaulike oscillations with a sufficiently long plateau phase.

To bring the 14D canonical model developed in [29] in accordance with the experimental conditions described above, we remove from the model the equations and terms describing blocked currents: I_{CaF}, I_{CaS}, and I_h. For simplicity, we assume that the partial block of outward currents completely removes I_{K1}, as well as I_{KA}, whereas it reduces I_{K2}. The current I_{NaP} is ignored for simplicity. The resulting model described in [11] reads as follows:

$$CV' = -(\bar{g}_{K2} m_{K2}^2 (V - E_K) + g_1 (V - E_1) + \bar{g}_{Na} f(-150, 0.0305, V)^3 h_{Na} (V - E_{Na})),$$

$$m'_{K2} = \frac{f(-83, 0.018 + V_{K2}^{shift}, V) - m_{K2}}{\tau_{K2}},$$

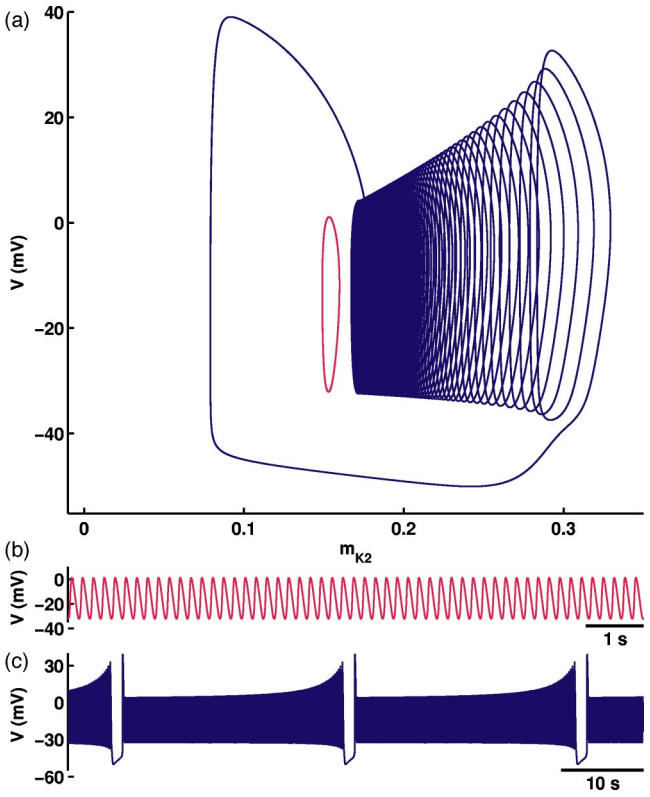

FIG. 2. (Color online) Coexistence of spiking and bursting modes in the model (1) in the (m_{K2},V)-projection for $V_{K2}^{shift}=-0.025\,98$ V. Initial conditions leading to tonic spiking and bursting are $(V,m_{K2},h_{Na})=(0.0,0.164,0.08)$ and (0.0, 0.165, 0.08), respectively. The small round periodic orbit in (a) corresponds to the tonic-spikes shown in (b); the larger, bursting cycle corresponds to the waveform shown in (c). The topology of bursting is illustrated in Figs. 3 and 5(d).

$$h'_{Na}=\frac{f(500,0.03391,\mathrm{V})-\mathrm{h}_{Na}}{\tau_{Na}}, \qquad (1)$$

where the variables V, m_{K2}, and h_{Na} are the membrane potential, activation of I_{K2}, and inactivation of I_{Na}, respectively. The parameters are the following: C is the membrane capacitance, $\bar{g}_{K2}$ is the maximum conductance of I_{K2}; E_K, and E_{Na} are the reversal potentials of K^+ and Na^+, respectively; $\bar{g}_{Na}$ is the maximal conductance of I_{Na}; g_1 and E_1 are the conductance and reversal potential of the leak current, respectively; τ_{K2} and τ_{Na} are the time constants of activation of I_{K2} and inactivation of I_{Na}, respectively; V_{K2}^{shift} is the shift of the membrane potential of half-inactivation of I_{K2} from its canonical value; and f is a Boltzman function: $f(x,y,z)=1/(1+e^{x(y+z)})$. The values of the parameters used in this study are $C=0.5$ nF, $\bar{g}_{K2}=30$ nS, $E_K=-0.07$ V, $E_{Na}=0.045$ V, $\bar{g}_{Na}=200$ nS, $g_1=8$ nS, $E_1=-0.046$ V, $\tau_{K2}=0.9$ s, and $\tau_{Na}=0.0405$ s. We use V_{K2}^{shift} as a bifurcation parameter.

One of the features of the model (1) is the bistability where stable tonic spiking coexists with the bursting mode, as shown in Fig. 2.

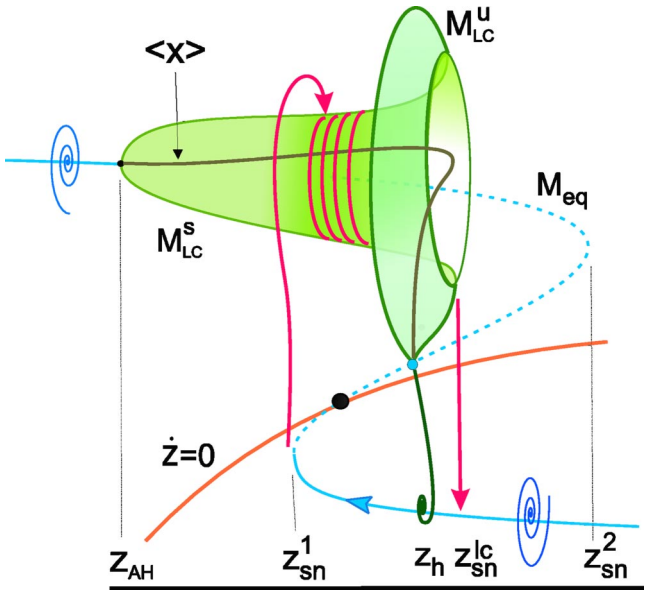

FIG. 3. (Color online) Bifurcation diagram of the fast subsystem in the (z,x)-extended phase plane. The curve M_{eq} consists of equilibrium points of the phase subsystem; its limit cycles span the surface M_{LC}. The curve $\langle x\rangle$ gives the average x coordinate of the limit cycles. The nullcline $\dot{z}=0$ crosses the unstable branch of M_{eq} at a single point corresponding to an unstable equilibrium state of the whole system. The arrowed curves outline the start and the end of a burst. The matching phase space of the neuron system (1) is presented in Fig. 5(d).

III. PHENOMENOLOGICAL DESCRIPTION

In the model (1), the time constant of the activation of the current I_{K2} is more than 20 times larger than those of the membrane potential V and inactivation of the current I_{Na}. Hence, we identify m_{K2} as the slow phase variable and V and h_{Na} as the fast ones. This allows us to consider (1) as a singularly perturbed system written in the following form:

$$\dot{x}=F(x,z), \quad \dot{z}=\mu G(x,z,\varepsilon), \qquad (2)$$

where $x\in\mathbb{R}^n(n\geqslant 2)$ and $z\in\mathbb{R}^1$ are the fast and the slow phase space variables, respectively, ε is a vector of control parameters, and $0<\mu\ll 1$. Both functions, F and G, are smooth enough, moreover, $G\equiv g(x,\varepsilon)-z$ as follows from the presentation of activation and inactivation variables of ionic currents according to Hodgkin-Huxley formalism.

When $\mu=0$, the fast and slow subsystems are decoupled. Now, the variable z serves as a governing parameter for the fast subsystem. The function F is assumed to satisfy some conditions typical for the system (1). They are illustrated in Fig. 3. The first one is that, depending on z, the fast subsystem has either one or three hyperbolic equilibrium states.

The coordinates of equilibria of the fast system are found from the equation $F(x,z)=0$ that defines a nullcline M_{eq} having a distinctive $\mathcal{Z}$-shape in projection onto the (z,x)-plane. The two turning points on M_{eq}, at z_{sn}^1 and z_{sn}^2, correspond to the saddle-node bifurcations in the fast subsystem where a pair of equilibrium states coalesce. In the interval $z_{sn}^1<z<z_{sn}^2$, the system (2) has three equilibria. The middle seg-

ment of M_{eq} is comprised of saddle points. The upper and lower branches of the nullcline M_{eq} correspond to the depolarized and hyperpolarized states of a neuron, respectively. The hyperpolarized (solid) branch of M_{eq} is comprised of stable equilibria of the fast subsystem. It is supposed that the stable focus on the upper branch becomes unstable through a generic (codimension-one) Andronov-Hopf bifurcation when z passes the critical value $z_{AH} < z^1_{sn}$. There are the two types of this bifurcation: sub- and supercritical. In the subcritical case, the stable focus becomes unstable when a repelling limit cycle collapses into it. If there are no other equilibrium states before z_{AH}, then this unstable cycle may only originate from a saddle-node bifurcation of limit cycles. This saddle-node bifurcation also generates a stable limit cycle that surrounds both the equilibrium state and the unstable limit cycle. In the supercritical case, the stable limit cycle emerges from the focus as z increases through the bifurcational value z_{AH}. In either case, the supercritical Andronov-Hopf bifurcation or the saddle-node bifurcation for limit cycles gives rise to the surface M^s_{LC} comprised solely of the stable limit cycles of the fast subsystem. The subsequent evolution of the stable limit cycle as z increases further can develop in two different ways. For example, the branch M^s_{LC} may terminate at a homoclinic bifurcation of the saddle point on the middle branch of M_{eq}, like in [22,23], i.e., the stable limit cycle becomes a homoclinic orbit of the saddle point with the negative saddle value, which is a sum of the characteristic exponents of the saddle point of the fast subsystem. Oppositely, if the saddle value is positive, then another, unstable limit cycle bifurcates from the homoclinic orbit as z increases through z_h, thereby constituting the "unstable" surface M^u_{LC}. Hence, as z approaches the value z^{lc}_{sn}, the stable and the unstable limit cycles get closer and merge finally into a double one at z^{lc}_{sn}.

This value corresponds to a saddle-node bifurcation for the limit cycles in the fast subsystem. The last scenario makes the united surface $M_{LC} = M^s_{LC} \cup M^u_{LC}$ look like it is turned inside out [see a sketch in Fig. 3 and its numerical reconstruction in Fig. 5(d)].

After the stable limit cycle has vanished in the saddle-node bifurcation at $z > z^{lc}_{sn}$, a neighboring phase point starts seeking another attractor [see Figs. 3 and 5(b)]. Such an attractor is the stable equilibrium state on the lower branch of M_{eq}. As the parameter z is now decreased, the phase point follows this hyperpolarized branch towards the low knee point at z^1_{sn}. The disappearance of this steady-state attractor for $z < z^1_{sn}$ triggers the phase point to switch back to the stable limit cycle on M^s_{LC}.

Next we discuss the dynamics of the whole, singularly perturbed system (2) when $0 < \mu \ll 1$. Introduce another nullcline $\dot{z} = 0$, which is the surface given by $G(x,z,\varepsilon) = 0$ (see Fig. 3). Let $\dot{z}$ be negative on M_{eq} wherever it is below the nullcline and positive above it. An intersection point of this nullcline with the nullcline M_{eq} (where $\dot{x} = 0$) is the equilibrium state of the whole system. To make the system exhibit bursting behavior, let this equilibrium state be unstable, i.e., be on the unstable (dotted) branch of M_{eq}. It follows from the works by Fenichel [30] that both surfaces, M_{eq} and M_{LC}, will persist as invariant manifolds for small enough μ as well. Moreover, each remains μ-close to the original wherever it is normally hyperbolic (e.g., far from bifurcations). Therefore, the phase point of the whole system will follow the same path in the (z,x)-phase space. Namely, it translates slowly along the lower branch of M_{eq} leftward until the fold. Then, it makes a rapid, vertical jump up onto the surface M_{LC}. Afterwards, it moves slowly rightward coiling around M_{LC}. Having reached the edge of M_{LC} at z^{lc}_{sn}, the phase point falls straight down onto M_{eq} to start a new cycle. Such trajectory behavior is associated with bursting in neuron models. The number of spikes in a burst is a number of complete revolutions of the phase point around M_{LC}.

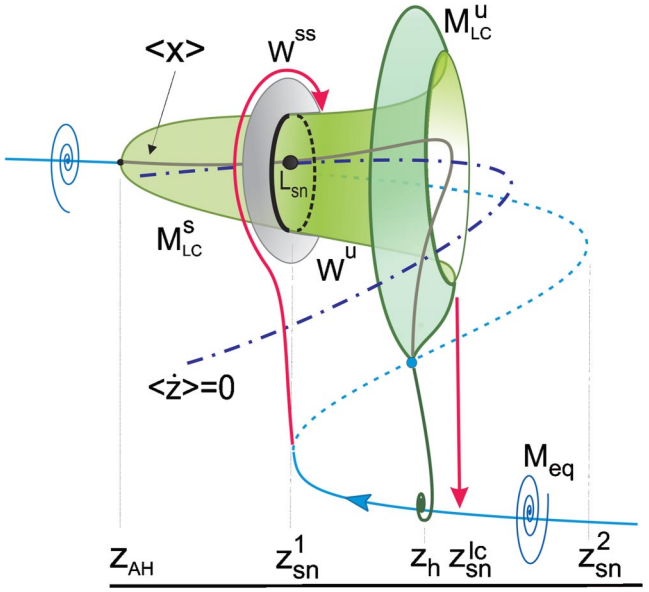

FIG. 4. (Color online) Tangency between the nullclines $\langle \dot{z} \rangle = 0$ and $\langle x \rangle$ makes a saddle-node periodic orbit L_{sn}. Its 2D unstable manifold W^u (composed of the segment of the surface M^s_{LC} between z^1_{sn} and z^{lc}_{sn} and the hyperpolarized branch of M_{eq}) comes back to the bifurcating orbit L_{sn} along the nonleading manifold W^{ss} (gray disk). The vertical vectors indicate the points of the fast jumps between the branches. This sketch is a singularly perturbed analog of Fig. 1.

In the following section we discuss the conditions under which the system has a stable periodic orbit on the surface M^s_{LC} that corresponds to tonic spiking. The presence of this orbit does not let the trajectories of the system, circulating around M^s_{LC}, pass throughout it.

Average nullclines and periodic orbits

The surface M_{LC} is composed of the limit cycles of the fast system at $\mu = 0$. Let us introduce the average value $\langle x \rangle$ of the x-coordinate of such a limit cycle $\varphi(t;z)$ with period $T(z)$ at given $z: \langle x(z) \rangle = [1/T(z)] \int_0^{T(z)} \varphi(t;z) dt$. By varying z, we define the corresponding continuous curve in the (z,x) space (see Fig. 4). Evidently, it originates at the Andronov-Hopf bifurcation at z_{AH} and terminates at the homoclinic bifurcation at z_h. The curve has a distinctive knee point at z^{lc}_{sn} corresponding to the saddle-node bifurcation of the stable and unstable limit cycles of the fast subsystem.

In the first approximation, the dynamics of the singularly perturbed system around M^s_{LC} is determined, by following "averaged" slow subsystem:

$$\dot{z} = \mu\langle G(z,\varepsilon)\rangle \equiv \frac{\mu}{T(z)}\int_0^{T(z)} G(\varphi(t;z),z,\varepsilon)dt. \qquad (3)$$

Hence, if $\langle G(z,\varepsilon)\rangle > 0$ within $z_{\rm sn}^1 \leqslant z \leqslant z_{\rm sn}^{\rm lc}$ at some ε, then the surface $M_{\rm LC}$ is transitive for solutions of the system (2) that coil around $M_{\rm LC}$ slowly (at the rate of $\sim\mu$) translating rightward.

Let some z^0 between $z_{\rm sn}^1$ and $z_{\rm sn}^{\rm lc}$ be a simple zero of the function $\langle G((z,\varepsilon))\rangle$ for some fixed ε. This zero is also an equilibrium state of this averaged slow subsystem. This equilibrium state is stable if $\langle G(z^0,\varepsilon)\rangle_z < 0$, or unstable otherwise. Then, as follows from Pontryagin-Rodygin theory [31], every zero of $\langle G\rangle$ corresponds to a periodic orbit of the whole singularly perturbed system. The stability of the periodic orbit in the x direction is determined by that of the corresponding limit cycle $M_{\rm LC}$ of the fast subsystem at the given z^0. Recall that the components $M_{\rm LC}^{\rm s}$ and $M_{\rm LC}^{\rm u}$ of $M_{\rm LC}$ are comprised of the stable and unstable limit cycle of the fast subsystem. Therefore, to study bifurcations of stable periodic orbits of the singulary perturbed system, we need to examine the upper branch of the curve $\langle x\rangle$ corresponding to the stable component $M_{\rm LC}^{\rm s}$.

Recall too that the function G is linear in z: $G(x,z,\varepsilon) = g(x,\varepsilon) - z$. Define an average nullcline $\langle\dot{z}\rangle = 0$ as the parametrically given curve

$$[z = \langle g(\zeta)\rangle,\ x = \langle x(\zeta)\rangle]$$

with

$$\langle g(\zeta)\rangle = [1/T(\zeta)]\int_0^{T(\zeta)} g(\varphi(t;\zeta),\varepsilon)dt$$

and $\langle x(\zeta)\rangle = [1/T(\zeta)]\int_0^{T(\zeta)}\varphi(t;\zeta)dt$. Any of its intersection points with the curve $\langle x\rangle$ [comprised of pairs $(z,\langle x(z)\rangle)$] correspond to a zero z^0 of $\langle G\rangle$, i.e., to a periodic orbit of our system. Note that if G is linear in both x and z, then the average nullcline $\langle\dot{z}\rangle = 0$ and the regular nullcline $\dot{z} = 0$ are the same curve. Evidently, this is not the general case. Furthermore, in contrast to the curve $\dot{z} = 0$, which can be found analytically, the analysis of the location and the shape of the average nullcline $\langle\dot{z}\rangle = 0$ in the (z,x) space requires numeric simulations. The corresponding average nullclines $\langle V\rangle$ and $\langle m'_{\rm K2}\rangle = 0$ of the neuron model (1) are shown in Figs. 4, 5(c), and 6 for different values of the bifurcation parameter $V_{\rm K2}^{\rm shift}$.

Next let us elaborate on how the average nullcline $\langle\dot{z}\rangle = 0$ may depend on the control parameter ε in the slow equation of the system. Suppose that ε be introduced so that the nullcline $\langle x\rangle = 0$ crosses the upper, stable branch of the curve $\langle x\rangle$ twice for some $\varepsilon > \varepsilon^*$. Then, these intersection points correspond to a pair of periodic orbits, one stable, $L_{\rm n}$, and one, $L_{\rm s}$, of the saddle type [see Figs. 5(a) and 5(c)]. By decreasing ε, the distance between the orbits decreases, and when the average nullcline $\langle x\rangle = 0$ has a tangency with the curve $\langle x\rangle$ at some ε^*, then the system possesses a saddle-node periodic orbit $L_{\rm sn}$, which vanishes for $\varepsilon < \varepsilon^*$ [see Fig. 5(d)]. Additionally, we require that $\langle G(z^0,\varepsilon^*)\rangle_\varepsilon \neq 0$. If so, the distance between the bifurcating periodic orbits is evaluated as $\sqrt{\varepsilon - \varepsilon^*}$. When $\varepsilon < \varepsilon^*$, i.e., there are no periodic orbits on $M_{\rm LC}^{\rm s}$, which becomes transitive, then the neuron exhibits solely bursting activity.

IV. BISTABILITY AND HOMOCLINIC SADDLE-NODE BIFURCATION

In order to reveal the origin of bistability, we continue to draw the parallels between the phenomenological description of bifurcations in the system (2) and the empirical studies of the neuron system (1). We will also discuss a mechanism that gives rise to the onset of chaos in the system. In both cases primary roles are played by the homoclinic bifurcations of the saddle and the saddle-node periodic orbits. Since the latter is the organizing center of our construction, let us start with its analysis first.

A spatial saddle-node periodic orbit has two unique manifolds, strongly stable $W^{\rm ss}$ and unstable $W^{\rm s}$; in the particular case of $\mathbb{R}^3$ both are of dimension two [32]. The strongly stable manifold $W^{\rm ss}$ breaks a vicinity of the saddle-node periodic orbit $L_{\rm sn}$ into two regions: node and saddle. In the node region, the saddle-node periodic orbit is stable, i.e., a trajectory converges to it as time tends to $+\infty$. In contrast, $L_{\rm sn}$ is repelling in the saddle region, where it has the unstable manifold $W^{\rm u}$ comprised of orbits converging to the saddle-node in backward time. We are interested in the global behavior of this unstable manifold, more specifically, whether it can be homoclinic, i.e., biasymptotic to the saddle-node periodic orbit. Recurrent behavior of the solutions of the slow-fast systems depicted in Fig. 2 supports this assertion.

In this paper, we consider a particular situation where the unstable manifold $W^{\rm u}$ of the saddle-node periodic orbit comes back to the orbit along the strongly stable manifold $W^{\rm ss}$ of the saddle-node periodic orbit $L_{\rm sn}$; see the sketch in Fig. 1.

The case where $W^{\rm u}$ comes back from the node region making infinitely many revolutions, the so-called blue-sky catastrophe, was discovered and analyzed for the neuron system (1) in [33]. Note that since an intersection of two surfaces in $\mathbb{R}^3$ is transverse, the presence of noncentral homoclinic connections to the saddle-node does not raise the codimension of the bifurcation. This bifurcation was first introduced and studied by Lukyanov and Shilnikov [34,35]. Let us elaborate on its basic properties. The unfolding of the bifurcation is sketched in Fig. 6. This bifurcation is best described by using a two-dimensional Poincaré map that is defined on some cross section transverse to the periodic orbits. The point where a periodic orbit hits the cross section is a fixed point of the Poincaré map. If the fixed point is stable, so is the corresponding periodic orbit. In the case of the saddle-node periodic orbit, there is a fixed point of the saddle-node type with a single multiplier equal to +1. So, when the saddle-node periodic orbit $L_{\rm sn}$ decomposes into the stable, $L_{\rm n}$, and the saddle, $L_{\rm s}$, periodic orbits, the corresponding saddle-node fixed point breaks into two points too: one stable and one fixed point of the saddle type. Let this occur above the corresponding bifurcation curve SN in Fig. 6. Because the saddle-node fixed point has noncentral homoclinic orbits generated by transverse crossings of its unstable and

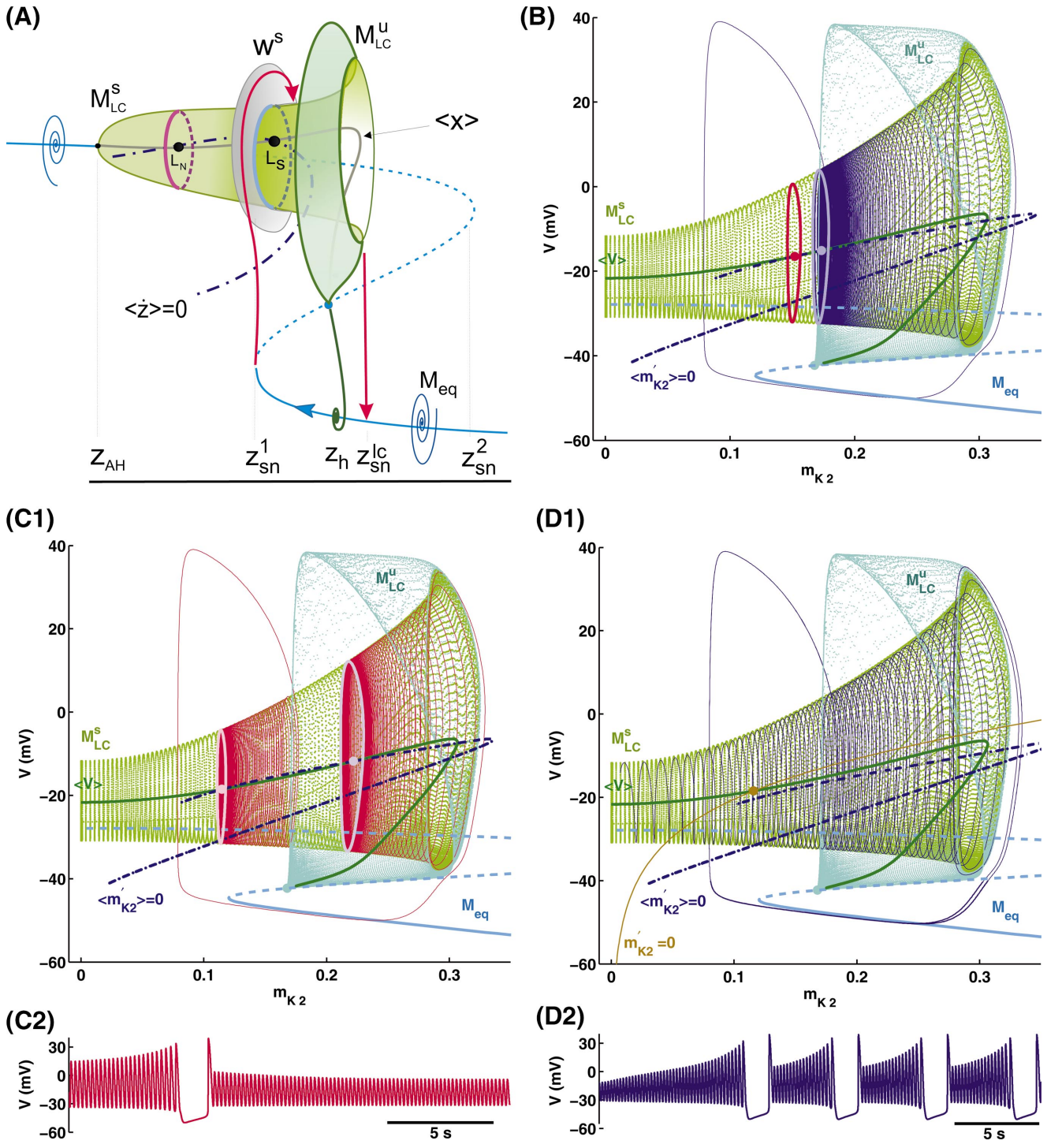

FIG. 5. (Color) (a) Intersection points of the average nullcline $\langle x\rangle=0$ with $\langle x\rangle$ yield one stable, $L_{\rm n}$, and one saddle, $L_{\rm n}$, periodic orbit of the singularly perturbed system. The stable manifold W^s of the saddle periodic orbit L_s bounds the attraction basin of L_n. This situation corresponds to (b) and inset 4 in Fig. 6. (b) Intersection points of the nullclines $\langle m'_{\rm K2}\rangle=0$ and $\langle V\rangle$ yield the stable and saddle periodic orbits of the neuron system (1). Compare to (a). The waveform of the bursting and tonic activities are shown in Fig. 2. (c) The saddle periodic orbit in ($C1$) no longer separates the basing of the bursting from the basing of the stable periodic orbit corresponding to the tonic spiking activity ($C2$) at $V^{\rm shift}_{\rm K2}=-0.027$ V. This type of behavior takes place to the left of the bifurcation curve B_2 (inset 2) in Fig. 6. (d) Geometry ($D1$) and the waveform ($D2$) of attracting bursting in the neuron model (1) at $V^{\rm shift}_{\rm K2}=-0.027$ V. The intersection point of the nullclines $m'_{\rm K2}=0$ and $M_{\rm eq}$ is the unstable equilibrium state of (1). The surface of $M_{\rm LC}$ is composed of the periodic orbits continued as the control parameter $V^{\rm shift}_{\rm K2}$ is varied. There is no intersection between the average nullclines $\langle m'_{\rm K2}\rangle=0$ and $\langle V\rangle$. Accordingly, the trajectory shown coils around $M_{\rm LC}$ translating rightwards and converges to the bursting attractor. Compare with Fig. 3.

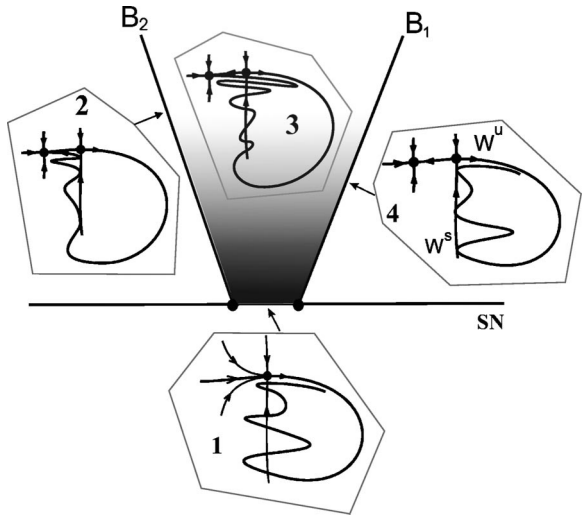

FIG. 6. (Color online) There are three principal bifurcation curves in the unfolding for the Lukyanov-Shilnikov bifurcation of a saddle-node fixed point with noncentral homoclinics (inset 1 showing the Poincaré map). The two bifurcation curves, B_1 and B_2, which are the boundaries of the darkened sector, correspond to the very first (inset 4) and last (inset 2) homoclinic tangencies between the stable, W^s, and unstable, W^u, sets of the saddle fixed point. The complex hyperbolic structure existing in this sector is due to transverse homoclinic crossings of these sets (inset 3). This structure will persist also after the disappearance of the saddle-node point beneath the segment indicated on the bifurcation curve SN.

strongly stable manifolds, it follows that after the splitting, the saddle point inherits the transverse homoclinic structure too. The presence of transverse homoclinic orbits implies the existence of Smale horseshoes, the abundance of saddle trajectories, and chaos, which persist even after the saddle-node disappears below the indicated sector. It is the main feature of saddle-node bifurcations of this kind.

Here, the stable L_n and saddle L_s periodic orbits coexist on the tube M^s_{LC}. Of special interest here is the right boundary B_1 (inset 4 in Fig. 6). This boundary corresponds to the first tangency between the stable W^s and unstable W^u manifolds of the saddle periodic orbit. To the right from B_1, the stable manifold W^s of the saddle orbit bounds the attraction basin of the stable periodic orbit. This situation corresponds to the coexistence of tonic spiking and bursting activities in the neuron, i.e., to bistability. Geometrically, the bistability in the dynamics of the system (2) takes place when the z^1_{sn}-coordinate of the left knee point on M_{eq} is on to the right from the saddle periodic orbit L_s on the surface M^s_{LC} [see Fig. 5(a)].

Let us return to consideration of the behavior of the solutions of the system 2 in the bistability sector between the bifurcation curves B_1 and B_2 in inset 3 of Fig 6.

In our phenomenological description, we assume that the phase point makes momentarily vertical jumps between the slow motion surfaces M_{eq} and M_{LC}. In the neuron model, the appearance of these jumps may vary between projections of the phase space (compare for example Figs. 2 and 9), presenting the (m_{K2}, V)- and $(m_{K2}, -h_{Na})$-phase portraits, respectively.

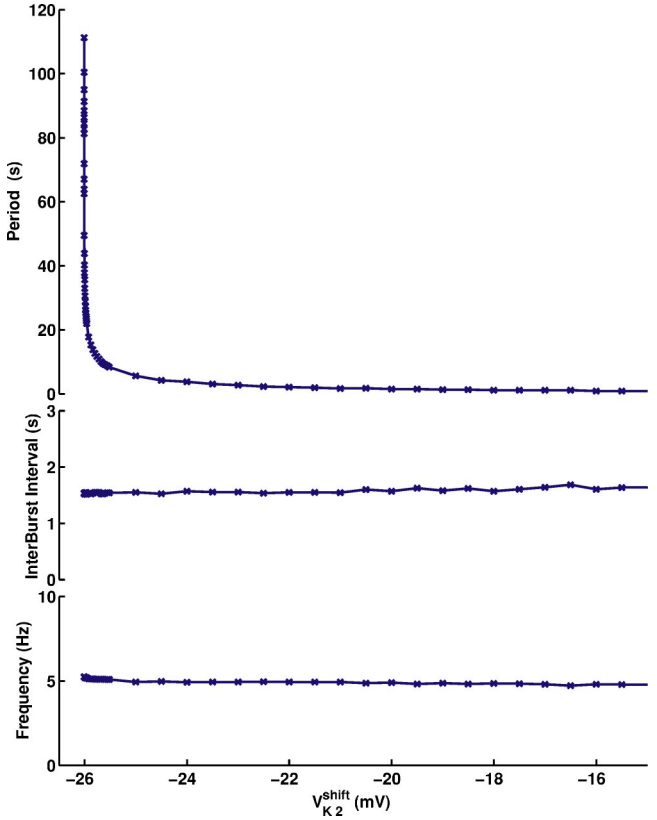

FIG. 7. (Color online) Temporal characteristics of bursting en route to spiking. The burst period (top chart) increases as $\sim|\ln(V^{shift}_{K2}+0.260\,086\,6)|$. The logarithmic fit of the burst duration in given in Fig. 8. Interburst interval (middle) and frequency of spikes (bottom) remain almost constant.

The bistability in the neuron model (1) is illustrated in Fig. 5(b). Depending on initial condition, the system may generate tonic spiking, if the initial point is in the attraction domain of the stable periodic orbit, or it generates bursting activity. The saddle periodic orbit separates these attraction domains. The knowledge of the topology of the solutions of the slow-fast system gives a clear intuition as to how different kinds of stimulations may switch operation of the neuron between the tonic spiking and bursting modes. The influence of stimulation on the slow variable, m_{K2}, is apparently most important. For the parameter regime presented in Fig. 5(b), if

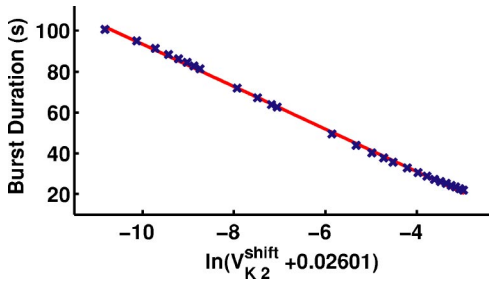

FIG. 8. (Color online) Logarithmic fit of the dependence of the burst duration on the control parameter V^{shift}_{K2}. Note that the burst duration obeys the same law because the interburst interval hardly changes within the indicated parameter interval.

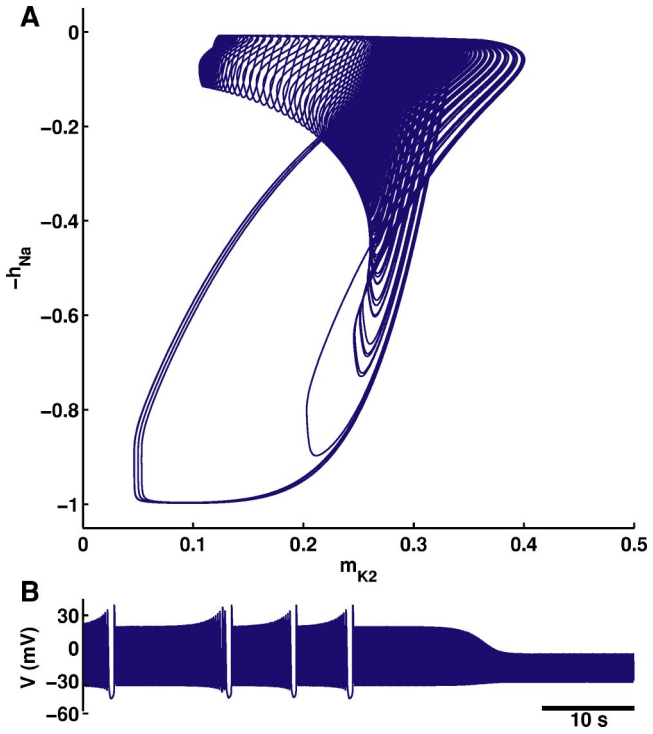

FIG. 9. (Color online) Intermittent transition to tonic spiking. A number of bursts are generated before the stable periodic orbit captures the phase point as illustrated in a projection to the $(-h_{\mathrm{Na}}, m_{\mathrm{K2}})$-phase plane (a) and as a voltage-time series (b). The model (1) is at control parameter $V_{\mathrm{K2}}^{\mathrm{shift}}=0.033\,67$ V. This intermittency corresponds to region (3) in Fig. 6.

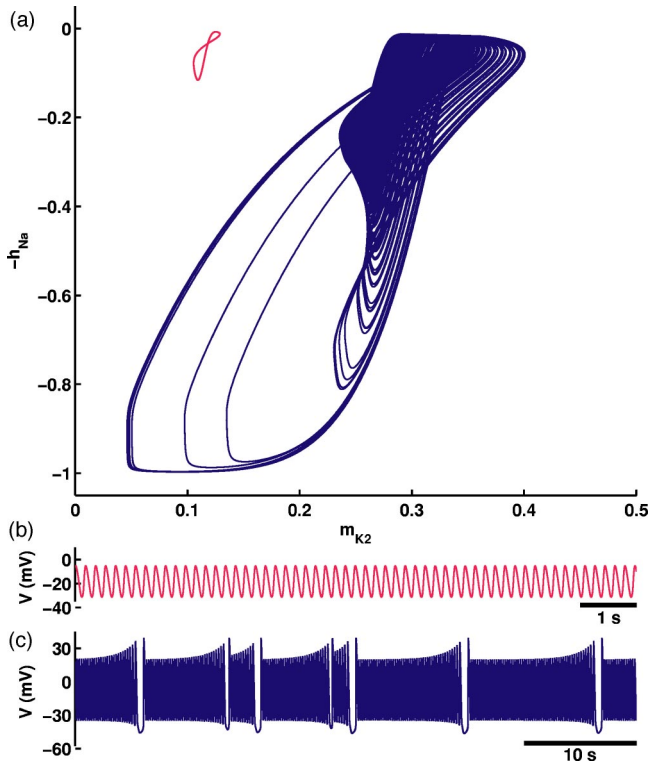

FIG. 10. (Color online) Chaotic bursting at $V_{\mathrm{K2}}^{\mathrm{shift}}=0.033\,670\,9$ V presented in a projection on the $(-h_{\mathrm{Na}}, m_{\mathrm{K2}})$ plane (a) and as a voltage-time series (b). Adjusting $V_{\mathrm{K2}}^{\mathrm{shift}}$ regularizes bursting as shown in Fig. 2.

m_{K2} is chosen below 0.16, the tonic spiking is observed, while the bursting occurs for values exceeding a threshold 0.17, provided the same initial values for V and h_{Na}.

When the control parameter $V_{\mathrm{K2}}^{\mathrm{shift}}$ is decreased, the stable and unstable periodic orbits move farther apart, so that the unstable manifold of the saddle orbit can no longer bound the attraction basin of the stable orbit where the phase point tends to as it jumps off the hyperpolarized phase of the bursting, as shown in Fig. 5(c). This situation corresponds to inset 2 in Fig. 6 on the left of the curve B_2. Here, the neuron may only exhibit tonic spiking.

Observe that the duration of bursting phase may grow with no bound as the control parameter is moved toward the transition value between the regimes, while the interburst interval remains nearly constant (see Figs. 7 and 8). The estimate for the growth of the burst period is given by $T(z,\alpha^*)|\ln(\alpha-\alpha^*)|$, where α^* is a deviation of a control parameter from the boundary B_1 into the bursting region, and $T(z,\alpha^*)$ is the period of the limit cycle on the surface M_{LC} of the fast subsystem at the given z. Note also that the bursting behavior is not necessarily regular here but can be chaotic as well, especially when the phase point may pass close by the stable periodic orbit (see Fig. 10).

On the left of the boundary B_2, the bistability ends so that the tonic spiking becomes the dominant regime. For the model (2), this situation occurs when the left knee point at z_{sn}^1 turns out to be to the left of the saddle periodic orbit L_{s} on $M_{\mathrm{LC}}^{\mathrm{s}}$. Any trajectory starting on the right of the stable manifold W^{s} of the saddle periodic orbit will get attracted to the stable one right after a single cycle of bursting (see inset 2 in Fig. 6). The corresponding phase space portrait of the neuron system (1) is shown in Fig. 5(c).

The intermittency in the system takes place between the boundaries B_1 and B_2 (see Inset 3 in Fig. 6). Here, the system may generate a train of bursting before it starts firing continuous spikes. The exact number of bursts and duration of each burst in the train are impossible to predict. This is another consequence of the complex shift dynamics due to homoclinic wiggles pictured in Fig. 6 (inset 3). Figure 10 shows a chaotic train composed of four bursts. The width of the parameter interval corresponding to the intermittency is small in a singularly perturbed system with $|\mu|\ll 1$. Furthermore, it is proportional to the diameter of the tube of the unstable manifold W^{u}, which is shrinking while it gets back to the saddle-node periodic orbit (see the sketch in Fig. 1). Recall that the low hyperpolarized branch of M_{eq} is comprised of the stable equilibria of the fast subsystem. In virtue of Liouville's theorem, a low estimate for volume compression can be given by $e^{(\mathrm{div}\,F+\mu)\tau}$, with $\tau\simeq(z_{\mathrm{sn}}^{\mathrm{lc}}-z_{\mathrm{sn}}^1)/\mu$ and $\mathrm{div}\,F<0$ on the low branch of $\mathrm{M_{eq}}$. So, if μ is small, so is the diameter of the tube of the unstable manifold W^{u} and, hence, is the size of the intermittency interval in the parameter space. This makes this kind of intermittency transition hard to find in a singular perturbed system. On the other hand, its presence can serve as indirect evidence that the system does not run on multiple time scales.

V. CONCLUSION

We propose a new general scenario of transition between tonic spiking and bursting. This mechanism also explains bistability in the system, where the bursting mode coexists with tonic spiking so that either mode can be attained by an appropriate choice of initial conditions. The core of the mechanism is based on a bifurcation of codimension one for a saddle-node periodic orbit with noncentral homoclinic orbits.

We identified this scenario in a leech neuron model (1). For the first time this bifurcation has been shown to occur in an autonomous model describing the dynamics of a physical entity. We argue that it is typical for slow-fast systems based on the Hodgkin-Huxley formalism. Moreover, we developed a geometrical framework for an averaging method of singularly perturbed systems. It constitutes a powerful tool for effective detection and bifurcation analysis of periodic orbits in neuron models.

Our description is not restricted to the given three-dimensional neuron model and holds for higher dimensions as well. Since the key bifurcation of the scenario is of codimension one, it may be revealed in electrophysiological experiments. The signatures of the key bifurcation are (1) coexistence of tonic spiking and bursting; (2) smooth transition between the two regimes; (3) logarithmic growth of the burst duration *en route* toward tonic spiking; and (4) chaotic intermittency of transient bursting turning into tonic spiking.

ACKNOWLEDGMENTS

We thank D. Turaev for helpful comments. The numeric analysis of system (1) utilized the software packages CONTENT [36]. A.S. acknowledges the RFBR Grants No. 02-01-00273, No. 05–01–00558 and No. 01-01-00975. G.C. and R.L.C. were supported by NIH Grant No. NS43098. A.S and G.C. appreciate a GSU internal research team and Brains and Behavior grants.

[1] E. Marder and R. L. Calabrese, Physiol. Rev. **76**, 687 (1996).
[2] M. Steriade, D. A. McCormick, and T. J. Sejnowski, Science **262**, 679 (1993).
[3] E. Izhikevich, N. Desai, E. Walcott, and F. Hoppensteadt, Trends Neurosci. **26**, 161 (2003).
[4] J. Lisman, Trends Neurosci. **20**, 38 (1997).
[5] J. Hartings, S. Temereanca, and D. Simons, J. Neurosci. **23**, 5264 (2003).
[6] P. Reinagel, D. Godwin, S. M. Sherman, and C. Koch, J. Neurophysiol. **81**, 2558 (1999).
[7] C. C. Canavier, D. A. Baxter, L. Clark, and J. Byrne. J. Neurophysiol. **69**, 2252 (1993).
[8] C. C. Canavier, D. A. Baxter, J. Clark, and J. Byrne, J. Neurophysiol. **72**, 872 (1994).
[9] R. Bertram, Biol. Cybern. **69**, 257 (1993).
[10] R. Butera, Chaos **8**, 274 (1998).
[11] G. S. Cymbalyuk and R. L. Calabrese. Neurocomputing **159**, 159 (2001).
[12] J. Hounsgaard and O. Kiehn, J. Physiol. (London) **414**, 265 (1989).
[13] H. Lechner, D. Baxter, C. Clark, and J. Byrne, J. Neurophysiol. **75**, 957 (1996).
[14] G. Turrigiano, E. Marder, and L. Abbott, J. Neurophysiol. **75**, 963 (1996).
[15] E. Marder, L. Abbott, G. Turrigiano, Z. Liu, and J. Golowasch, Proc. Natl. Acad. Sci. U.S.A. **26-93**(24), 13481 (1996).
[16] X. J. Wang, Neuroscience **59**(1), 21 (1994).
[17] E. Izhikevich, J. Bifurcation Chaos **10**(6), 1171, (2000).
[18] J. Rinzel, Lect. Notes Math. **1151**, 304 (1985).
[19] J. Rinzel, Lect. Notes Biomath. **71**, 267 (1987).
[20] V. N. Belykh, I. V. Belykh, M. Colding-Joregensen, and E. Mosekilde, Eur. Phys. J. E **3**, 205, (2000).
[21] E. Mosekilde, B. Lading, S. Yanchuk, and Yu. Maistrenko, BioSystems **63**. 3 (2001).
[22] D. Terman, J. Nonlinear Sci. **2**, 135 (1992).
[23] X. J. Wang, Physica D **62**, 263 (1993).
[24] B. Doiron, C. Laing, and A. Longtin, Comp. Neurosci. **12**, 5 (2002).
[25] B. Deng and G. Hines, Chaos **12**, 533 (2002).
[26] A. L. Hodgkin and A. F. Huxley, J. Physiol. (London) **117**, 500 (1952).
[27] G. S. Cymbalyuk, Q. Gaudry, M. A. Masino, and R. L. Calabrese J. Neurosci. **22**, 10580, 2002.
[28] C. A. Opdyke and R. L. Calabrese, J. Comp. Physiol. **175**, 781 (1994).
[29] A. Hill, J. Lu, M. Masino, O. Olsen, and R. L. Calabrese, J. Comput. Neurosci. **10**, 281 (2001).
[30] N. Fenichel, J. Diff. Eqns. **31**, 53 (1979).
[31] L. S. Pontryagin and L. V. Rodygin, Sov. Math. Dokl. **1**, 611 (1960).
[32] L. Shilnikov, A. Shilnikov, D. Turaev, and L. Chua, *Methods Qualitative Theory in Nonlinear Dynamics*, Vol. I (World Scientific, Singapore, 1998), Vol. II (2001).
[33] A. Shilnikov and G. Cymbalyuk, Phys. Rev. Lett. **94**, 048101 (2005).
[34] V. Lukaynov and L. Shilnikov, Sov. Math. Dokl. **19**(6), 1314 (1978).
[35] A. Shilnikov, L. Shilnikov, and D. Turaev, Mosc. Math. J. **5**(1), 205 (2005).
[36] CONTENT is available at ftp://ftp.cwi.nl/pub/CONTENT.
[37] G. Cymbalyuk and A. L. Shilnikov, J. Comput. Neurosci. **18**(3), 255 (2005).